Turbulent flow of a gas-solid suspension through a channel

Sourav Ganguli[1,*], *Partha S.* Goswami[2], and *Manaswita* Bose[1]

[1]Department of Energy Science and Engineering, Indian Institute of Technology Bombay, Powai, Mumbai, 400076, India
[2]Department of Chemical Engineering, Indian Institute of Technology Bombay, Powai, Mumbai, 400076, India.

Abstract. The objective of the present work is to study the flow of gas-solid suspension in planar channels of finite dimensions using a coupled Large Eddy Simulations-Discrete Element Model (LES-DEM) approach. Dynamic k-equation subgrid scale model (DKSGS) is used to compute the fluctuations in the subgrid-scale. First, the simulation is performed for a vertical channel with periodicity in the spanwise direction in order to compare the results with the Direct Numerical Simulation- Hard sphere (DNS-HS) simulations. Second, the simulation is performed for vertical channels with confined span, in which the wall effect along spanwise and cross-stream directions is investigated. Each term of the kinetic energy and momentum balance equations is computed to understand the significance of individual effects at different solid concentrations within the channel. Simulations are performed for Re of 3300 and particle Stokes numbers of 32 and 105. It is observed that the nature of attenuation of the turbulent intensity depends on the grid selection,n even though particle free flow is grid converged.

1 Introduction

Gas-solid flow is common in nature and industrial applications. In the case of particle-laden flow, the interaction of particles with fluid and interparticle collision play important roles in the overall flow behavior. In wall-bounded flows, specifically for pneumatic transport through vertical and horizontal ducts or pipes, the influence of particle concentration and inertia on turbulence augmentation or attenuation is studied experimentally [1, 2]. For particles with higher inertia, the formation of the wake behind individual particles enhances the turbulence intensity, and the drag force due to the relative motion of the particles with respect to the fluid causes turbulence attenuation [3, 4]. Tanaka and Eaton [5] defined a non-dimensional number i.e. Particle momentum number (Pa_{St}) based on particle Stokes number (St), fluid bulk Reynolds number (Re) and Kolmogorov length scale (χ) to classify flow regimes for turbulence augmentation and attenuation.

Numerical simulations are performed for particle-laden flows considering one, two, and four-way coupling depending on the solid concentration in the flow [3]. Four way coupling is considered for sufficiently high solid volume fraction ($\phi_s \geq 10^{-3}$). A drastic decrease in the turbulence intensity due to the sudden reduction in the rate of turbulent energy production at a critical value of solid concentration (ϕ_s) is observed in the coupled DNS-HS simulations with perfectly smooth particles by Muramulla et al. [6]. This phenomenon is termed a catastrophic turbulence collapse. Later, Rohilla et al. [7, 8] performed a simulation on the configuration of Muramulla et al. [6] using spectral-LES and FVM-LES. Simulations [9, 10] are also performed to resolve fluid-particle interaction in order to capture particle-generated wakes using the immersed boundary method. However, this method is significantly computationally intensive and yet to be used for large systems.

The main objective of the present study is to simulate the flow of gas-solid suspension through vertical duct using coupled LES-DEM techniques as implemented in OpenFOAM and LIGGGHTS. The objective also includes investigating the influence of channel walls along the spanwise direction on the profiles of the mean and the fluctuating properties of the particle-free and the particle-laden fluid flow.

2 Methodology

Figure 1 shows a schematic of the channel with dimensions $L : h : W = 4 : 4\pi : 1$. In case of the spanwise periodic channel, the dimensions are: $2/3\pi : 4\pi : 1$. Fluid phase turbulence is modeled using LES. The Dynamic k-equation subgrid Scale (DKSGS) model [11] is used to determined the residual kinetic energy ($K_{sgs} = \frac{1}{2}(\widetilde{U_i'^2} - U_i^2)$). Governing equations for the fluid and the particle phase with the constitutive relations are presented in Equations 1 to 5. Here, U' and U represent the fluid instantaneous and filtered velocity. The mean and fluctuating part of the filtered velocity is represented as $\overline{U}$ and $u.\widetilde{\ }$ is used to represent the filtering operation. "p" represents the filtered pressure. The dissipation term of residual kinetic energy (ϵ) depends on the model coefficient C_ϵ and grid resolution ($\overline{\Delta}$). Fluid density and kinematic viscosity are represented as ρ_f and ν_f.

*e-mail: sourav.research.123@gmail.com

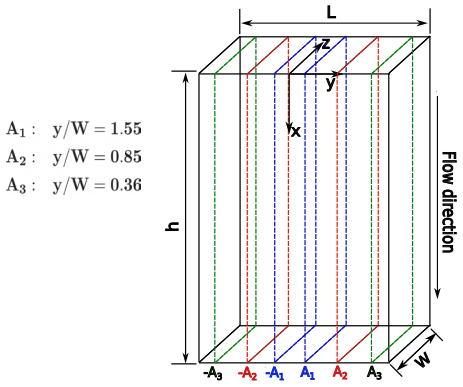

Figure 1: Schematic of downward flow through spanwise confined channel; A_1, A_2, and A_3 are the off-center planes on which the profiles are determined, in addition to the center plane

$$\frac{\partial U_i}{\partial t} + \frac{\partial \widetilde{U_i' U_j'}}{\partial x_j} = \nu_f \frac{\partial^2 U_i}{\partial x_j \partial x_j} - \frac{\partial \tau_{ij}^r}{\partial x_j} - \frac{1}{\rho_f}\frac{\partial p}{\partial x_i} \quad (1)$$

$$\frac{\partial k_{sgs}}{\partial t} + U_i \frac{\partial k_{sgs}}{\partial x_i} = -\tau_{ij}\frac{\partial U_i}{\partial x_j} - \epsilon + \frac{\partial}{\partial x_i}\left(\nu_T \frac{\partial k_{sgs}}{\partial x_i}\right) \quad (2)$$

$$\epsilon = C_\epsilon \frac{\sqrt{k_{sgs}}}{\overline{\Delta}} \quad (3)$$

$$m\frac{\mathrm{d}\mathbf{v}}{\mathrm{d}t} = \mathbf{F}_c + \mathbf{F}_D + \mathbf{F}_b + \mathbf{F}_g + \mathbf{F}_L \quad (4)$$

$$F_c \hat{n} = -k_n \boldsymbol{\delta}_n \quad (5)$$

Here, m, d_p, ρ_P, and $\mathbf{v}$ are the mass, diameter, density, and velocity of individual particles. $\mathbf{F}_b$ and $\mathbf{F}_g$ represent the buoyancy force and the body force. F_c represents the contact force due to interparticle or wall particle collision. The linear spring-dashpot model [12] is used to determine the contact force $\mathbf{F}_c$, where k_n represent the spring stiffness along the radial or normal direction of contact. Schiller-Naumann model for drag ($\mathbf{F}_D = 3\pi\mu_f d_P(\mathbf{U}-\mathbf{v})(1 + 0.15Re_p^{0.687})$) and Saffman lift force ($\mathbf{F}_L = 1.61 {d_P}^2 \sqrt{\rho_f \mu_f}\,|\nabla\times\mathbf{U}|^{-1/2}(\mathbf{U}-\mathbf{v})\times(\nabla\times\mathbf{U})$,[3]) are used to determine the fluid-particle interaction. Particles used in the simulations are inertial with Stokes numbers 32 and 105 [13]. The bulk Reynolds number is set at 3300. All simulations are performed using open-source software CFDEM (OpenFOAM coupled with LIGGGHTS). Simulations are performed using two different grids: G1 ($z+_{\text{first point}} = 0.35$, stretch ratio = 28), and G2 ($z+_{\text{first point}} = 0.31$, stretch ratio = 15) to compare the results with DNS (direct numerical simulation, [6]. Simulations are performed in both spanwise periodic and confined channels. Parameters are selected from the cases presented in [6]. Table 1 lists different nondimensional numbers [6] for the bulk Re of 3300, where $\mathrm{Re_p}$ and Fr represent particle Reynolds number and Froude number. u_t represents the single particle terminal velocity.

Table 1: Relevent nondimensional number used for comparing the simulation results with DNS-HS outcome [6]

ρ_P/ρ	$\mathrm{Re_P}$	Fr	$\mathrm{d_P/h}$	χ/h	$\mathrm{u_t/U_b}$	St
520	60	1197	1.85×10^{-2}	0.0023	0.035	32
1690	60	1197	1.85×10^{-2}	0.0023	0.063	105

3 Simulation result

3.1 Validation of particle-free flow with DNS result

Figure 2 shows the comparison of the profiles of mean fluid velocity ($\overline{U}_x$) with the DNS results of [6]. The mean velocity profile has an excellent agreement with the DNS results for both G1 and G2. $\overline{u_x u_x}$ also shows a very good agreement with the DNS results. The peak value of $\overline{u_x u_x}$ obtained using LES in a spanwise periodic and confined channel differs from DNS results by [6] only by 3% and 6%, respectively. The agreement between the DNS and LES results is poor for $\overline{u_x u_z}$ and $\overline{u_z u_z}$. The mismatch between $\overline{u_x u_z}$ at the central plane profile of the confined channel and that in the periodic channel could be due to the interplay of the terms in the momentum and the energy balance equations.

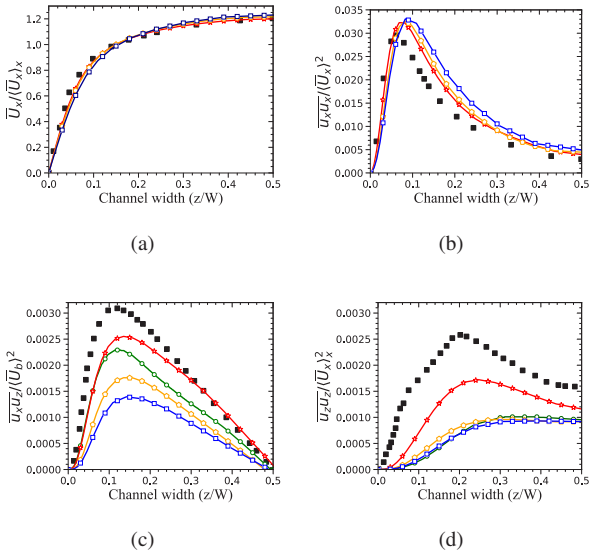

Figure 2: Variation of normalized $\overline{U}_x$, $\overline{u_x u_x}$, $\overline{u_x u_z}$ and $\overline{u_z u_z}$ along the channel width (z/W) for LES on G1 (-o-) and G2 (-☆-) in a spanwise periodic channel and G1 (-□-) and G2 (-⬠-) in confined channel, and DNS result (■) [6]

We next study the effect of the confining walls in the spanwise direction on the fluid phase profiles. Fluid mean velocity ($\overline{U}_x$) and second moment of fluid fluctuating velocity i.e. $\overline{u_x u_x}$, $\overline{u_x u_z}$ and $\overline{u_z u_z}$ are shown in Figure 3 at three different spanwise locations in addition to the central plane ($\frac{y}{W} = \pm0.36, \pm0.85, \pm1.55$). In a channel with aspect ratio 1:4, these positions are ±9%, ±21%, ±38.75% of the half spanwise position. The results show that the confining walls have marginal effects on the profiles of $\overline{U}_x$, $\overline{u_x u_x}$, and $\overline{u_x u_z}$ up to ~ 20% from the central plane. The profile of $\overline{u_z u_z}$ shows no effect of the wall up to ±9%(±20d_p) from the central plane. These results suggest that the profiles at the central plane in a channel with an aspect ratio of 1:4, are not influenced by the presence of walls in the larger dimension. We next investigate the particle-laden flow.

3.2 Particle laden flow

Figure 4 shows the comparison for profiles of $\overline{U}_x$, $\overline{u_x u_x}$, $\overline{u_x u_z}$, $\overline{u_z u_z}$ for St = 105 and mass loading ratio,

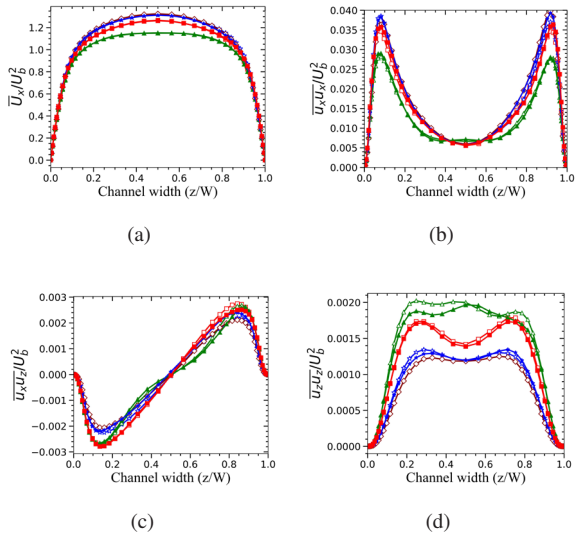

Figure 3: Variation of (a) $\overline{U}_x$ normalized by U_b, (b) $\overline{u_x u_x}$, (c) $\overline{u_x u_z}$ and (d) $\overline{u_z u_z}$ normalized by U_b^2 along the channel width (z/W) for different planes along y-direction; $-\mathrm{A}_1$ (-△-), $-\mathrm{A}_2$(-□-), $-\mathrm{A}_3$ (-☆-), $y/W = 0$ (-◇-), A_3 (-★-), A_2 (-■-), A_1 (-▲-); A_1 ($y/W = 1.55$), A_2 ($y/W = 0.85$), A_3 ($y/W = 0.36$)

MR = 0.845 obtained from LES-DEM and DNS-HS. Profiles of $\overline{U_x}$ and $\overline{u_x u_x}$ have very good agreement with DNS-HS [6]. The peak value of the $\overline{u_x u_x}$ and $\overline{u_x u_z}$ from LES-DEM are 9% and 15% different from the DNS-HS. The agreement on $\overline{u_z u_z}$ is not good; however, the value of $\overline{u_z' u_z'}$ is $O(10^{-1})$ smaller than $\overline{u_x u_x}$. The particle mean velocity ($\overline{v}_x$) has an excellent agreement near the centre of the channel; however, the slip is more in DNS-HS than LES-DEM. The average mean mass flow rate of solid particles in LES-DEM differs by 3% from DNS-HS due to the numerical error. $\overline{v_x' v_x'}$ and $\overline{v_z' v_z'}$ is higher in case of LES-DEM. Also, cross-correlation term $\overline{v_x' v_z'}$ is higher in LES-DEM than DNS-HS. The mean and the fluctuating energy balance of the fluid phase is examined as a consistency check. Eqn. 6 and Eqn.7 are fluid phase the mean and the fluctuating energy balance integrated over the cross-stream dimension.

$$\langle -\overline{U_x}\frac{\partial \overline{p}}{\partial x}\rangle - \langle \mu_f \left(\frac{\partial \overline{U_x}}{\partial z}\right)^2\rangle - \langle \rho_f \widetilde{\overline{u_x u_z}}\frac{\partial \overline{U_x}}{\partial z}\rangle - \langle \overline{U_x}\left(\overline{K_{fs} n_p (U_x - v_x)}\right)\rangle = 0 \quad (6)$$

$$\langle \rho_f \widetilde{\overline{u_x u_z}}\frac{\partial \overline{U_x}}{\partial z}\rangle - \langle \sum_{i=x,y,z}\sum_{j=x,y,z} 2\mu_f \left(\frac{\partial u_j}{\partial i} s_{ij}\right)\rangle - \langle D_f\rangle = 0 \quad (7)$$

$$D_f = \overline{K_{fs} n_p U_x (U_x - v_x)} + \overline{K_{fs} n_p U_y \left(U_y - v_y\right)} + \overline{K_{fs} n_p U_z (U_z - v_z)} - \overline{U_x}\left(\overline{K_{fs} n_p (U_x - v_x)}\right) \quad (8)$$

Here $\langle\rangle$ represents channel height averaged quantities ($\langle\bigstar\rangle = \int_0^1 \bigstar d(z/W)$). $\langle \overline{U_x}\frac{\partial \overline{p}}{\partial x}\rangle$ and $\langle \mu_f \left(\frac{\mathrm{d}\overline{U}_x}{\mathrm{d}z}\right)^2\rangle$ represent pressure work and work done by the viscous stress for the mean scale. Figure 5 represents the pointwise variation of

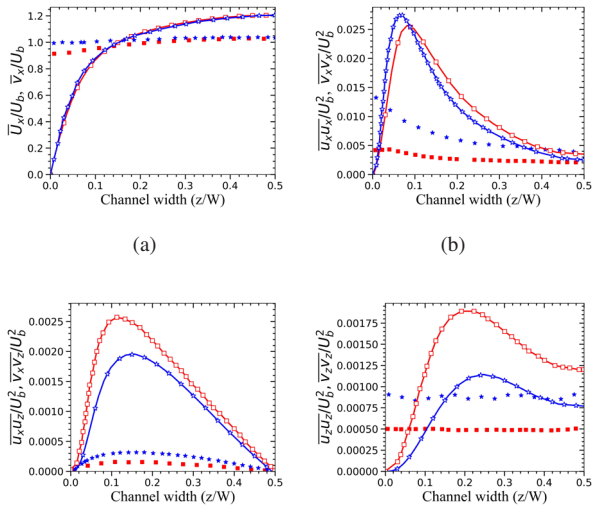

Figure 4: Comparison of fluid (-□-, -☆-) and particle phase (■, ★) (a) mean velocity and (b,c,d) stress components for Muramulla et al. [6] and current simulation results for particle stokes number of 105

different terms of energy balance equation before taking avarage over channel height.

$\langle -\overline{\rho u_x u_z}\left(\frac{\mathrm{d}\overline{U}_x}{\mathrm{d}z}\right)\rangle$ represents the turbulence energy production due to residual stress. $\langle -\overline{U}_x\overline{\left(K_{fs} n_p (U_x - v_x)\right)}\rangle$ represents the work done by drag force where K_{fs} and n_p represents the momentum exchange coefficient and number density of the particles. $\langle \sum_{i=x,y,z}\sum_{j=x,y,z} 2\mu_f \left(\overline{\frac{\partial u_j}{\partial i} s_{ij}}\right)\rangle$ represents viscous energy dissipation for the fluctuating kinetic energy. The last term D_f represents the work done due to the fluctuating drag force (Eqn. 8). Different terms of Eqn. 6, ★, are plotted as a function of the channel height in Fig. 5. The maximum point-residual is of $O\left(10^{-1}\right)$. The residual of the height averaged balance equations (6 and 7) are of $O\left(10^{-3}\right)$.

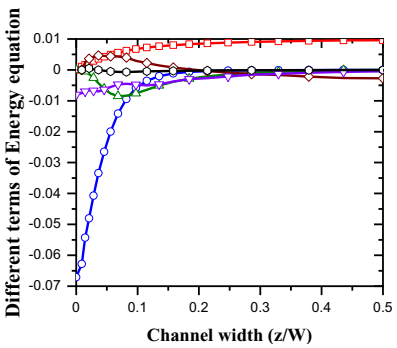

Figure 5: Energy equation terms: $-\overline{U}_x\left(\frac{\mathrm{d}\overline{p}}{\mathrm{d}x}\right)$ (-□-), $\mu_f\left(\frac{\mathrm{d}\overline{U}_x}{\mathrm{d}z}\right)^2$ (-◇-), $-\overline{\rho u_x u_z}\left(\frac{\mathrm{d}\overline{U}_x}{\mathrm{d}z}\right)$ (-○-), $-\overline{U}_x\overline{\left(K_{fs} n_p (U_x - v_x)\right)}$ (-▽-), $\mu_f \frac{\mathrm{d}}{\mathrm{d}z}\left(\overline{U}_x \frac{\mathrm{d}\overline{U}_x}{\mathrm{d}z}\right)$ (-☆-) and D_f (-◁-) for MR of 0.845 (ϕ_s is 5×10^{-4})

3.3 Turbulence attenuation

Figure 6 shows the simulation results for particle Stokes number 32 for spanwise periodic downward channel flow. The mass loading ratio (MR) is varied from 0.1 to 1.5. The second moment of fluid fluctuating velocity i.e. $\overline{u_x u_x}$, $\overline{u_x u_z}$ (Fig. 6a, 6b) gradually decreases with the increase of solid concentration. In contrary, a catastrophic turbulence collapse due to the drastic reduction in the turbulence production term $-\overline{\rho u_x u_z}\left(\frac{\mathrm{d}\overline{U}_x}{\mathrm{d}z}\right)$ is reported in [6–8]. Muramulla et al. [6] observed the collapse at a critical solid volume fraction, $\phi = 10^{-3}$ for Re = 3300 and St = 32 using DNS-HS. Early collapse of turbulence was reported in [7, 8] for simulations performed using LES-HS and LES-DEM. They have reasoned that the error associated with the estimation of the turbulent kinetic energy in the subgrid scale modelling approach causes the early collapse.

In the current work, performed for exactly the same case as [6], the turbulence intensity decreases with the increase of solid concentration, though a sudden collapse of turbulence intensity is not observed, contradicting the results of Rohilla et al. [7]. To our surprise, a significant reduction in turbulence intensity, consistent with the results reported in [6] is observed with a coarser spanwise grid. This discrepancy requires further investigation.

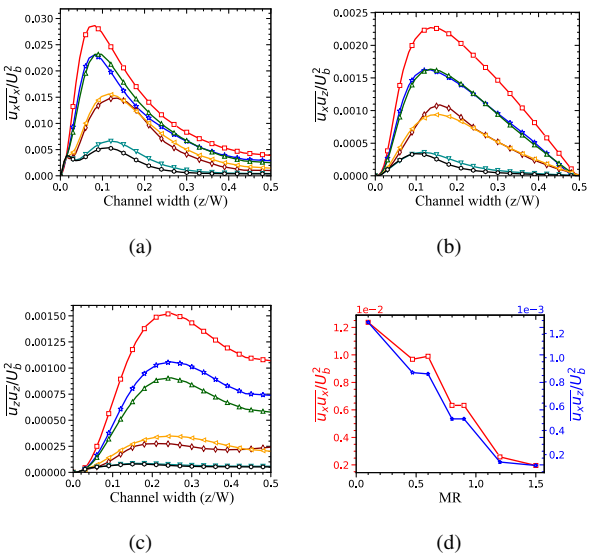

Figure 6: Variation of (a) $\overline{U}_x$ normalized by U_b and (b) fluid stresses i.e. $\overline{u_x u_x}$ and (c) $\overline{u_x u_z}$ normalized by U_b^2 along the channel width (z/W) for solid to fluid mass loading ratio of 0.1 (–□–), 0.47 (–☆–), 0.6 (–△–), 0.8 (–◇–), 0.9 (–◁–), 1.2 (–▽–) and and 1.5 (–○–), and (d) channel width averaged fluid second moments i.e. $\langle\overline{u_x u_x}\rangle_z/U_b^2$ (–□–) and $\langle\overline{u_x u_z}\rangle_z/U_b^2$ (–☆–) for different MR

4 Conclusion

The Dynamic k-equation subgrid scale (DKSGS) model was used to simulate the downward flow of turbulent gas-solid suspension through vertical channels. Two types of channels were considered: one with periodicity in the spanwise direction and one with the confining wall. The confined channel has an aspect ratio of 1:4. As a first step, the results from the particle-free simulations were compared with the DNS simulations. The grid was selected based on the comparison. The effect of the confining walls on the mean profiles of the $\overline{U_x}$, $\overline{u_x u_x}$, $\overline{u_x u_z}$, $\overline{u_z u_z}$ was investigated. It was found that the profiles at the central plane are not influenced by the presence of the wall. Particle laden flows are simulated with $\mathrm{Re}_{\mathrm{Bulk}} = 3300$ and St = 32, 105. The fluid mean profiles are in good agreement with the DNS-HS results. The particle phase shows a higher fluctuation in the case of LES-DEM. Simulations were also carried out for different mass-loading ratios (MR). Turbulence intensity is gradually reduced for the increase of MR to 1.2 ($\phi = 2.3 \times 10^{-3}$). In summary, this work reports the comparison between the LES-DEM and DNS-HS results for the transportation of turbulent gas-solid suspension; however, more systematic analyses are required to understand the reasons behind the disagreement in the cross-stream moments.

References

[1] Y. Tsuji, et al., J. Fluid Mech. **120**, 385–409 (1982).
[2] S. Elghobashi, et al., Phys. Fluids A **5**, 1790 (1993).
[3] C.T. Crowe, Multiphase flow handbook (CRC press, 2005)
[4] S. Balachandar, et al., Annu. Rev. Fluid Mech. **42**, 111 (2010).
[5] T. Tanaka, et al., Phys. Rev. Lett. **101**, 114502 (2008).
[6] P. Muramulla, et al., J. Fluid Mech. **889**, A28 (2020).
[7] N. Rohilla, et al., Phys. Rev. Fluids **7**, 024302 (2022).
[8] N. Rohilla, et al., Physics of Fluids **35**, 053323 (2023).
[9] M. Uhlmann, , Physics of Fluids **20** (2008).
[10] M. Uhlmann, J. Dušek, Int. J. Multiph. Flow **59**, 221 (2014).
[11] W.W. Kim, et al., in *33rd aerospace sciences meeting and exhibit* (1995), p. 356
[12] J.Schafer, et al., , J. Phys. I France **6**, 5 (1996).
[13] L. Brandt, et al., Annu. Rev. Fluid Mech. **54**, 159 (2022).